AIChE

# Study of Effect of Temperature Gradient on Solid Dissolution Process under Action of Transverse Rotating Magnetic Field

**Rafał Rakoczy**
Institute of Chemical Engineering and Environmental Protection Process, West Pomeranian University of Technology, 71-065 Szczecin, Poland

*DOI 10.1002/aic.12656*
*Published online June 28, 2011 in Wiley Online Library (wileyonlinelibrary.com).*

*The study of effect of the transverse rotating magnetic field on the dissolution process of rock-salt sample is the main purpose of this work. Moreover, the experimental study of the influence of the temperature gradient between the surface of sample and the solvent temperature on this process is presented in this article. The results of investigations are worked out by means of the novel type dimensionless equations including standard and magnetic numbers. The obtained results are compared with the data given in the previous literature.* © 2011 American Institute of Chemical Engineers *AIChE J,* 58: 1030–1039, 2012
*Keywords: mass transfer, dissolution process, heat transfer, transverse rotating magnetic field*

## Introduction

The design, scale-up, and optimization of industrial processes conducted in agitated systems require, among other, precise knowledge of the hydrodynamics, mass- and heat-transfer parameters, and reaction kinetics. Literature data available indicate that the mass-transfer process is generally the rate-limiting step in many industrial applications. Because of the tremendous importance of mass-transfer in engineering practice, a very large number of studies have determined mass-transfer coefficients both empirically and theoretically. From the practical point of view, the agitated systems are usually used to dissolve granular or powdered solids into a liquid solvent.[1]

One of the key aspects in the dynamic behavior of the mass-transfer processes is the role of hydrodynamics. On a macroscopic scale, the improvement of hydrodynamic conditions can be achieved by using various techniques of mixing, vibration, rotation, pulsation, and oscillation in addition to other techniques such as the use of fluidization, turbulence promotes or magnetic and electric fields, and so on. The transverse rotating magnetic field (TRMF) is a versatile option for enhancing several physical and chemical processes. Studies over the recent decades were focused on application of magnetic field (MF) in different areas of engineering processes.[2,3] Static, rotating, or alternating MFs might be used to augment the process intensity instead of mechanically mixing. The practical applications of MF are presented in the relevant literature.[4–13]

Recently, the TRMF are widely used to control different processes in the various engineering operations.[14–16] This kind of MF induces a time-averaged azimuthal force, which drives the flow of the electrical conducting fluid in circumferential direction. According to information available in the technical literature, the mass-transfer during the solid dissolution to the surrounding liquid under the action of the TRMF has been deliberated.[2,3]

It should be noticed that the temperature gradient induces buoyancy-driven convective flow in the fluid. This temperature gradient has a significant practical interest to the mass transfer process. It is reported that the difference

Correspondence concerning this article should be addressed to R. Rakoczy at rrakoczy@zut.edu.pl.

between the surface temperature of solid sample and the liquid temperature has strong influence on the dissolution process.[17]

The main objective of this study is to investigate the solid dissolution process that is induced under the action of the TRMF and the gradient temperature between solid surface and liquid. According to the information available in the technical literature, the usage of the TRMF and gradient temperature is not theoretically and practically analyzed. The obtained experimental data are generalized by using the empirical dimensionless correlations.

## Theoretical Background

### *Influence of TRMF on solid dissolution process*

Under forced convective conditions, the mathematical description of the solid dissolution process may be described by means of the differential equation of mass balance for the component $i$

$$\frac{\partial \rho_i}{\partial \tau} + \mathrm{div}(\rho_i \overline{w_i}) = \Phi_i \tag{1}$$

where $\Phi_i$ is the mass flux of component $i$ (the volumetric mass source of component $i$).

Taking into consideration the flux density of component $i$ $\left(\overline{J_i} = \rho_i \overline{w_i}\right)$ and the diffusion flux density $\left(\overline{J_{dyf}} = \rho_i (\overline{w_i} - \overline{w})\right)$, we obtain the following relation between $\overline{J_i}$ and $\overline{J_{dyf}}$

$$\overline{J_i} = \overline{J_{dyf}} + \rho_i \overline{w} \;\Rightarrow\; \rho_i \overline{w_i} = \rho_i (\overline{w_i} - \overline{w}) + \rho_i \overline{w} \tag{2}$$

Including the relation (2) in the Eq. 1 gives the relationship for the mass balance of component $i$

$$\frac{\partial \rho_i}{\partial \tau} + div\left[\overline{J_{dyf}}\right] + div(\rho_i \overline{w}) = \Phi_i$$
$$\Rightarrow \frac{\partial \rho_i}{\partial \tau} + div\left[\overline{J_{dyf}}\right] + (\rho_i \, div(\overline{w}) + \overline{w}\,\mathrm{grad}(\rho_i)) = \Phi_i \tag{3}$$

Taking into account the concentration of component $i$ ($c_i = \rho_i \rho^{-1} \Rightarrow \rho_i = \rho c_i$), we find the modified form of the Eq. 3

$$\frac{\partial(\rho c_i)}{\partial \tau} + \overline{w}\,\mathrm{grad}(\rho c_i) + (\rho c_i)\, div(\overline{w}) + div\left[\overline{J_{dyf}}\right] = \Phi_i \tag{4}$$

Equation 4 may be rewritten by

$$\rho \frac{\partial c_i}{\partial \tau} + \rho \overline{w}\,\mathrm{grad}(c_i) + c_i \left[\frac{\partial \rho}{\partial \tau} + \overline{w}\,\mathrm{grad}(\rho) + \rho\,\mathrm{div}(\overline{w})\right] + \mathrm{div}\left[\overline{J_{dyf}}\right] = \Phi_i \tag{5}$$

The term in square brackets is the so-called continuity equation, and the relation (5) may be simplified in the following form

$$\rho \frac{\partial c_i}{\partial \tau} + \rho \overline{w}\,\mathrm{grad}(c_i) + \mathrm{div}\left[\overline{J_{dyf}}\right] = \Phi_i \tag{6}$$

The total diffusion flux density $\left(\overline{J_{dyf}}\right)$ may be expressed as a sum of elementary fluxes considering the concentration $\left(\overline{J_i}(c_i)\right)$ and the additional force interactions $\overline{J_i}(\overline{F})$ (e.g., forced convection as a result of fluid mixing).

$$\overline{J_{dyf}} = \overline{J_i}(c_i) + \overline{J_i}(\overline{F}) \;\Rightarrow\; \overline{J_{dyf}} = -\rho D_i \,\mathrm{grad}(c_i) + \rho D_i k_{\overline{F}} \overline{F} \tag{7}$$

Under the action of the TRMF, the force $\overline{F}$ may be defined as the Lorentz force $\overline{F_{em}}$. This force is acting as the driving force for the liquid rotation, and it may be described by

$$\overline{F_{em}} = \left(\sigma_e \left(\overline{w} \times \overline{B}\right)\right) \times \overline{B} \tag{8}$$

Introduction of Eq. 8 in Eq. 7 gives the following relationship

$$\overline{J_{dyf}} = -\rho D_i \,\mathrm{grad}(c_i) + D_i k_{\overline{F_{em}}} \left(\left(\sigma_e \left(\overline{w} \times \overline{B}\right)\right) \times \overline{B}\right) \tag{9}$$

Taking into account the Eq. 9, we obtain the following general relationship for the mass balance of component $i$

$$\frac{\partial c_i}{\partial \tau} + \overline{w}\,\mathrm{grad}(c_i) + \mathrm{div}[-D_i \,\mathrm{grad}(c_i)] + \mathrm{div}\left[\frac{D_m}{\rho}((\sigma_e(\overline{w} \times \overline{B})) \times \overline{B})\right] = \frac{\Phi_i}{\rho} \tag{10}$$

It should be noticed that the coefficient of magnetic diffusion $D_m$ may be expressed as follows:

$$D_m = D_i k_{\overline{F_{em}}} \tag{11}$$

This coefficient may be defined by means of the following expression

$$D_m = c_i \tau_d \;\Rightarrow\; D_m = c_i \sigma_e \mu_m l_0^2 \;\Rightarrow\; D_m = \frac{c_i l_0^2}{\nu_m} \tag{12}$$

Taking into consideration the Eq. 12, we obtain the relationship

$$\frac{\partial c_i}{\partial \tau} + \overline{w}\,\mathrm{grad}(c_i) + \mathrm{div}[-D_i \,\mathrm{grad}(c_i)] + div\left[\frac{c_i l_0^2}{\nu_m \rho}\left(\left(\sigma_e \left(\overline{w} \times \overline{B}\right)\right) \times \overline{B}\right)\right] = \frac{\Phi_i}{\rho} \tag{13}$$

The above relation (Eq. 13) may be treated as the differential mathematical model of the solid dissolution process under the action of the TRMF. The right side of this equation represents the source mass of component $i$

$$\Phi_i = -\frac{\beta_i dF_m}{dV}(c_i - c_r) \Rightarrow\; \Phi_i = -(\beta_i)_V (c_i - c_r)$$
$$\Rightarrow\; \Phi_i = -(\beta_i)_V \widetilde{c_i} \;\Rightarrow \Phi_i = (\beta_i)_V (-\widetilde{c_i}) \tag{14}$$

where $(-\widetilde{c_i})$ is the driving force for the solid dissolution process.

Introduction of the Eq. 14 in the relation (13) gives the following relationship

$$\frac{\partial c_i}{\partial \tau} + \overline{w}\,\mathrm{grad}(c_i) + \mathrm{div}[-D_i\,\mathrm{grad}(c_i)] + \mathrm{div}\left[\frac{c_i l_0^2}{\nu_m \rho}\left(\left(\sigma_e\left(\overline{w}\times\overline{B}\right)\right)\times\overline{B}\right)\right] = -\frac{(\beta_i)_V\,\widetilde{c_i}}{\rho} \quad (15)$$

Taking into account the below definition of the dimensionless parameters

$$c_i^* = \frac{c_i}{c_{i_0}};\ \widetilde{c_i}^* = \frac{\widetilde{c_i}}{c_{i_0}};\ \overline{w}^* = \frac{\overline{w}}{w_0};\ D_i^* = \frac{D_i}{D_{i_0}};\ \tau^* = \frac{\tau}{\tau_0};\ \mu_m^* = \frac{\mu_m}{\mu_{m_0}};$$
$$\nu_m^* = \frac{\nu_m}{\nu_{m_0}};\ \rho^* = \frac{\rho}{\rho_0};\ \overline{B}^* = \frac{\overline{B}}{B_0};\ \left[(\beta_i)_V\right]^* = \frac{(\beta_i)_V}{\left[(\beta_i)_V\right]_0}$$
$$div^* = \frac{\mathrm{div}}{l_0^{-1}};\ Div^* = \frac{\mathrm{div}}{l_0^{-1}};\ \mathrm{grad}^* = \frac{\mathrm{grad}}{l_0^{-1}}; \quad (16)$$

we obtain the governing Eq. 16 in a symbolic form

$$\frac{c_{i_0}}{\tau_0}\left[\frac{\partial c_i^*}{\partial \tau^*}\right] + \frac{c_{i_0} w_0}{l_0}\left[\overline{w}^*\,\mathrm{grad}^*\left(c_i^*\right)\right] - \frac{D_{i_0} c_{i_0}}{l_0^2}\left[\mathrm{div}^*\left[D_i^*\,\mathrm{grad}^*\left(c_i^*\right)\right]\right] + \frac{c_{i_0}\sigma_{e_0} w_0 B_0^2 l_0}{\nu_{m_0}\rho_0}\left[\mathrm{div}^*\left[\frac{c_i^*}{\nu_m^*\rho^*}\left(\left(\sigma_e^*\left(\overline{w}^*\times\overline{B}^*\right)\right)\times\overline{B}^*\right)\right]\right] = -\frac{\left[(\beta_i)_V\right]_0 c_{i_0}}{\rho_0}\left[\frac{\left[(\beta_i)_V\right]^*\widetilde{c_i}^*}{\rho^*}\right] \quad (17)$$

The nondimensional form of this equation may be scaled against the convective term $\left(\frac{c_{i_0} w_0}{l_0}\right)$. The dimensionless form of Eq. 17 may be given as follows

$$\frac{l_0}{\tau_0 w_0}\left[\frac{\partial c_i^*}{\partial \tau^*}\right] + \left[\overline{w}^*\,\mathrm{grad}^*\left(c_i^*\right)\right] - \frac{D_{i_0}}{l_0 w_0}\left[\mathrm{div}^*\left[D_i^*\,\mathrm{grad}^*\left(c_i^*\right)\right]\right] + \frac{\sigma_{e_0} B_0^2 l_0^2}{\nu_{m_0}\rho_0}\left[\mathrm{div}^*\left[\frac{c_i^*}{\nu_m^*\rho^*}\left(\left(\sigma_e^*\left(\overline{w}^*\times\overline{B}^*\right)\right)\times\overline{B}^*\right)\right]\right] = -\frac{\left[(\beta_i)_V\right]_0 l_0}{\rho_0 w_0}\left[\frac{\left[(\beta_i)_V\right]^*\widetilde{c_i}^*}{\rho^*}\right] \quad (18)$$

This relation includes the following dimensionless groups characterizing the dissolution process under the action of TRM

$$\frac{l_0}{\tau_0 w_0} \Rightarrow S^{-1} \quad (19a)$$

$$\frac{D_{i_0}}{l_0 w_0} \Rightarrow \left(\frac{\nu}{w_0 D}\right)\left(\frac{D_{i_0}}{\nu}\right) \Rightarrow \mathrm{Re}^{-1}\mathrm{Sc}_i^{-1} \Rightarrow \mathrm{Pe}_i^{-1} \quad (19b)$$

$$\frac{\sigma_{e_0} B_0^2 l_0^2}{\nu_{m_0}\rho_0} \Rightarrow \left(\frac{\sigma_{e_0} B_0^2 l_0^2}{\nu\rho_0}\right)\left(\frac{\nu}{\nu_{m_0}}\right) \Rightarrow \mathrm{Q}\,\mathrm{Pr}_m \Rightarrow \mathrm{Ha}^2\,\mathrm{Pr}_m \quad (19c)$$

$$\frac{\left[(\beta_i)_V\right]_0 l_0}{\rho_0 w_0} \Rightarrow \left(\frac{\left[(\beta_i)_V\right]_0 d_p^2}{\rho_0 D_{i_0}}\right)\left(\frac{\nu}{w_0 D}\right)\left(\frac{D_{i_0}}{\nu}\right)\left(\frac{D^2}{d_s^2}\right) \Rightarrow \mathrm{Sh}\,\mathrm{Sc}^{-1}\mathrm{Re}^{-1}\left(\frac{D^2}{d_s^2}\right) \quad (19d)$$

Taking into account the definition of the nondimensional numbers (Eqs. 19a–19d), we find the following dimensionless governing equation

$$\mathrm{S}^{-1}\left[\frac{\partial c_i^*}{\partial \tau^*}\right] + \left[\overline{w}^*\,\mathrm{grad}^*\left(c_i^*\right)\right] - \mathrm{Pe}_i^{-1}\left[\mathrm{div}^*\left[D_i^*\,\mathrm{grad}^*\left(c_i^*\right)\right]\right] + \mathrm{Ha}^2\,\mathrm{Pr}_m\left[\mathrm{div}^*\left[\frac{c_i^*}{\nu_m^*\rho^*}\left(\left(\sigma_e^*\left(\overline{w}^*\times\overline{B}^*\right)\right)\times\overline{B}^*\right)\right]\right] = -Sh\ Sc^{-1}Re^{-1}\left(\frac{D^2}{d_s^2}\right)\left[\frac{\left[(\beta_i)_V\right]^*\widetilde{c_i}^*}{\rho^*}\right] \quad (20)$$

From the dimensionless form of the Eq. 20, it follows that

$$Sh\ Sc^{-1}Re^{-1}\left(\frac{D^2}{d_s^2}\right) \sim \mathrm{Ha}^2\,\mathrm{Pr}_m$$
$$\Rightarrow\ Sh\ Sc^{-1} \sim \mathrm{Ha}^2 Re\,\mathrm{Pr}_m\left(\frac{d_s^2}{D^2}\right)$$
$$\Rightarrow Sh\ Sc^{-1} \sim \mathrm{Ta}_m\mathrm{Pr}_m\left(\frac{d_s^2}{D^2}\right) \quad (21)$$

Under convective conditions, a relationship for the mass-transfer similar to the relationships obtained for heat-transfer may be expected of the form[18]

$$Sh = f(Re,\ Sc) \quad (22)$$

The two-principle dimensionless groups of relevance to mass-transfer are Sherwood and Schmidt numbers. The Sherwood number can be viewed as describing the ratio of convective to diffusive transport and finds its counterpart in heat-transfer in the form of the Nusselt number.[1]

The Schmidt number is a ratio of physical parameters pertinent to the system. This dimensionless group corresponds to the Prandtl number used in heat-transfer. Moreover, this number provides a measure of the relative effectiveness of momentum and mass transport by diffusion.

Reynolds number is added to these two groups, which represents the ratio of convective-to-viscous momentum transport. This number determines the existence of laminar or turbulent conditions of fluid flow. For small values of the Reynolds number, viscous forces are sufficiently large relative to inertia forces. However, with increasing the Reynolds number, viscous effects become progressively less important relative to inertia effects.

Evidently, for Eq. 22 to be of practical use, it must be rendered quantitative. This may be done by assuming that the functional relation is in the following form[19,20]

$$Sh = a_1 Re^{b_1} Sc^{c_1} \quad (23)$$

The mass-transfer coefficients in the mixed systems can be correlated by the combination of Sherwood, Reynolds, and Schmidt numbers. Using the proposed relation (23), it has been found possible to correlate a host of experimental data for a wide range of operations. The coefficients of relation (23) are determined from experiment. Under forced convection conditions, the relation may be expressed as follows[21]

$$Sh \sim Re^{0.5} Sc^{0.33} \quad (24)$$

The exponent on of the Schmidt number is to be 0.33[22–26] as there is some theoretical and experimental evidences for this value,[27] although reported values vary from 0.56[28] to 1.13.[29]

Mass transfer process under the TRMF conditions is very complicated and may be described by the nondimensional Eq. 20. Taking into account that the magnetic Prandtl number $Pr_m = \text{const}$ and the ratio of the diameters solid sample and the container diameter $\frac{d_s}{D} = \text{idem}$, the obtained relationship (see Eq. 21) may be expressed as follows

$$Sh\ Sc^{-1} \sim Ta_m Pr_m \left(\frac{d_s^2}{D^2}\right) \Rightarrow Sh = f(Ta_m, Sc) \tag{25}$$

### *Influence of temperature gradient on the solid dissolution controlled process*

As mentioned above, the temperature gradient has strong influence on the solid dissolution process. The heat transfer from the sample to the ambient fluid may be modeled by means of the well-known Nusselt-type equation $Nu = f(Re, Pr)$.

In the present report, we consider the process dissolutions described by a similar but somewhat modified relationship between the dimensionless Sherwood number and the numbers that are defined the intensity of the magnetic effects in the tested experimental set-up with the TRMF generator. It should be assumed that the relationship for the heat transport under the TRMF conditions can be characterized in the following general form $Nu = f(Ta_m, Pr)$.

The solid dissolution process under the action of the TRMF and the gradient temperature between the solid surface and the liquid may be described by means of the following equations system

$$\begin{cases} Sh = a_1 Ta_m^{b_1} Sc^{c_1} \\ Nu = a_2 Ta_m^{b_2} Pr^{c_2} \end{cases} \tag{26}$$

From Eq. 26, the ratio of Sherwood and Nusselt numbers is given by

$$\frac{Sh}{Nu} = a_3 Ta_m^{b_3} \left(\frac{Sc}{Pr}\right)^{c_3} \tag{27}$$

where $a_1 \neq a_2 \wedge a_3 = \frac{a_1}{a_2}$; $b_1 \neq b_2 \wedge b_3 = b_1 - b_2$; and $c_1 = c_2 \wedge c_3 = 0.33$.

In the relevant literature, the ratio of the Schmidt and Prandtl numbers is called as the dimensionless Lewis number (the ratio of thermal diffusivity to mass diffusivity)

$$Le = \left(\frac{Sc}{Pr}\right) Le = \left(\frac{\nu}{D_i}\right)\left(\frac{a}{\nu}\right) \Rightarrow Le = \frac{a}{D_i} \tag{28}$$

According to the Eq. 28 and the above assumptions, the ratio of Sherwood and Nusselt numbers is defined as follows

$$\frac{Sh}{Nu} = a_3 Ta_m^{b_3} Le^{0.33} \tag{29}$$

## Experimental Details

### *Experimental setup*

All experimental measurements of mass-transfer process using the TRMF were carried out in a laboratory setup including electromagnetic field generator. A schematic representation of the experimental apparatus is presented in the Figure 1.

This setup may be divided into: a generator of the rotating electromagnetic field (1), a glass container (2) with the conductivity samples (3 and 4), an electric control box (5) and an inverter (6) connected with multifunctional electronic switch (8), and a personal computer (7) loaded with special software. This software made possible the electromagnetic field rotation control, recording working parameters of the generator and various state parameters. The more detailed description of the experimental set-up is given in the previous article.[2]

The values of the magnetic induction at different points inside the glass container are detected by using a Hall sample connected to the personal computer. The typical example of the dependence between the spatial distributions of magnetic induction and the various values of the alternating current frequency for the cross-section of container is given.[30] The obtained results in this article suggest that the averaged values of magnetic induction may be analytically described by the following relation

$$[B_{\mathrm{TRMF}}]_{\mathrm{avg}} = 14.05[1 - \exp(-0.05 f_{\mathrm{TRMF}})] \tag{30}$$

### *Rock-salt sample heated by means of the cartridge heater*

In the case of these experimental investigations, the gradient temperature between the surface and liquid was caused by using the cartridge heater (power $\sim$ 1200 W). This tubular device was inserted into drilled holes of rock-salt sample for heating. The preparation procedure of the rock-salt sample is thoroughly described in previous publication.[2]

The heating setup contained the temperature controller and sensors. Sensors for the temperature control were placed

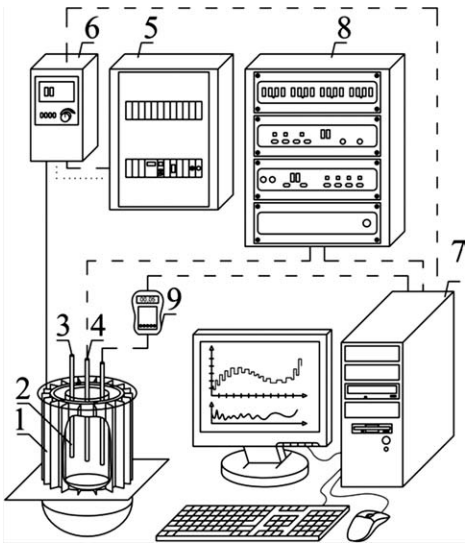


**Figure 1. Sketch of experimental setup.**

(1) Generator of rotating magnetic field, (2) glass container, (3,4) conductivity samples, (5) electronic control box, (6) a.c. transistorized inverter, (7) personal computer, (8) multifunctional electronic switch, and (9) Hall sample.

between the working surface of the sample and the heater. These sensors were also located on the surface of the solid sample. The sketch of rock-salt sample with the heating setup is graphically presented in the Figure 2. The sample was kept at a constant temperature (65, 70, or 80°C). The heat transfer from the sample to ambient fluid was realized for the various temperatures (20, 40, and 60°C). The system of temperature sensors was used to control the temperature of the water during the solid dissolution process.

### *Calculation of mass transfer coefficient*

The mass transfer coefficient under the action of the TRMF may be calculated form the following equation

$$-\frac{dm_i}{d\tau}=\beta_i F_m \widetilde{c_i} \Rightarrow \beta_i=\frac{1}{F_m(-\widetilde{c_i})}\frac{dm_i}{d\tau} \tag{31}$$

Equation 31 cannot be integrated because the area of solid body, $F_m$, is changing in time of dissolving process. It should be noted that the change in mass of solid body in a short time period of dissolving is very small, and the mean area of dissolved cylinder may be used. The relation between loss of mass, mean area of mass-transfer, and the mean driving force of this process for the time of dissolving duration is approximately linear, and then, the mass-transfer coefficient may be calculated from the simple linear equation

$$[\beta_i]_{\text{avg}}=\frac{1}{[F_m]_{\text{avg}}[\widetilde{c_i}]_{\text{avg}}}\frac{(-\text{dif}\, m_i)}{(\text{dif}\,\tau)} \tag{32}$$

The averaged surface $F_m$ is defined as follows

$$[F_m]_{\text{avg}}=\pi[d_s]_{\text{avg}}h_s \tag{33}$$

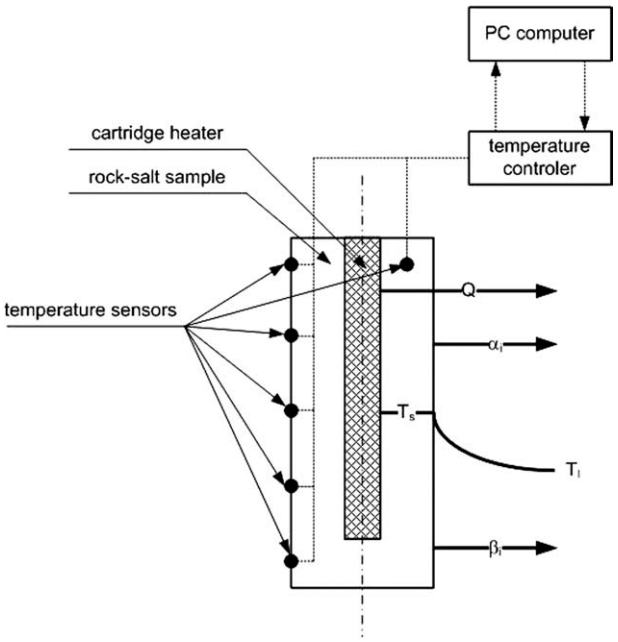


**Figure 2. Sketch of rock-salt sample with the heating setup.**

The volumetric mass transfer coefficient $(\beta_i)_V$ in Eq. 34 is described by relation

$$(\beta_i)_V=\frac{\beta_i dF_m}{dV} \;\Rightarrow\; \left[(\beta_i)_V\right]_{avg}=\frac{[\beta_i]_{\acute{s}r}[F_m]_{\acute{s}r}}{V_l} \tag{34}$$

### *Calculation of heat transfer coefficient*

The heat transfer from the sample to liquid may by modeled by the following relationship

$$Q_s=Q_l \;\Rightarrow\; \alpha_s F_m \Delta T_1=m_l c_{p_l}\Delta T_2 \tag{35}$$

This equation can be rewritten as

$$\alpha_s F_m\left(T_s-[T_l]_{t_2}\right)=m_l c_{p_l}\left([T_l]_{t_2}-[T_l]_{t_1}\right) \;\Rightarrow\; \alpha_s = \frac{m_l c_{p_l}\left([T_l]_{t_2}-[T_l]_{t_1}\right)}{F_m\left(T_s-[T_l]_{t_2}\right)} \tag{36}$$

and the averaged heat transfer coefficient is given as follows

$$[\alpha_s]_{\text{avg}}=\frac{m_l\left[c_{p_l}\right]_{\text{avg}}\left([T_l]_{t_2}-[T_l]_{t_1}\right)}{[F_m]_{\text{avg}}\left(T_s-[T_l]_{t_2}\right)} \tag{37}$$

The averaged coefficient of heat transfer ($[\alpha_s]_{\text{avg}}$) varies with the parameters of the TRMF mixing process and depends on the operating conditions and physical properties of the liquid.

## Results and Discussion

Under the TRMF conditions, a relationship for the mass-transfer can be described in the general form $Sh = f(Ta_m, Sc)$. The results of experiments suggest that the Sherwood number, the magnetic Taylor number, and the Schmidt number may be defined as follows

$$Sh=\frac{\left[(\beta_i)_V\right]_0 d_p^2}{\rho_0 D_{i_0}} \Rightarrow Sh=\frac{\left(\frac{[\beta_i]_{\acute{s}r}[F_m]_{\acute{s}r}}{V_l}\right)d_p^2}{\rho_l D_{i_l}} \tag{38a}$$

$$Sc_i=\frac{\nu}{D_{i_0}} \Rightarrow Sc_i=\frac{\nu_l}{D_{i_l}} \tag{38b}$$

$$Ta_m=Ha^2 Re_m \Rightarrow Ta_m=\left(\frac{\sigma_{e_0}B_0^2 l_0^2}{\nu\,\rho_0}\right)\left(\frac{w_0 D}{\nu}\right)$$

$$\Rightarrow Ta_m=\left(\frac{\sigma_{e_l}\left([B_{\text{TRMF}}]_{\text{avg}}\right)^2 D^2}{\nu_l\,\rho_l}\right)\left(\frac{\omega_{\text{TRMF}}D^2}{\nu_l}\right)$$

$$\Rightarrow Ta_m=\frac{\omega_{\text{TRMF}}\left([B_{\text{TRMF}}]_{\text{avg}}\right)^2 D^4\sigma_{e_l}}{\nu_l^2\rho_l} \tag{38c}$$

The above dimensionless groups (Eqs. 38a–38c) were calculated with the physical properties in the temperature range 20–60°C (the liquid temperature).

The effect of dissolution process under the action of the TRMF can be described by using the variable $ShSc^{-0.33}$ proportional to the term $a(Ta_m)^b$. The experimental results obtained in this work are graphically illustrated in $\log(ShSc^{-0.33})$ vs. $\mathrm{Log}(a(Ta_m)^b)$ in the Figure 3. Moreover, the influence of the temperature gradient between the surface temperature of solid and the liquid temperature on the mass transfer coefficient is presented in this figure.

To establish the effect of all important parameters on the dissolution process in the analyzed setup, we propose the following relationship to work out the experimental database

$$\frac{Sh}{Sc^{0.33}} = a(Ta_m)^b \tag{39}$$

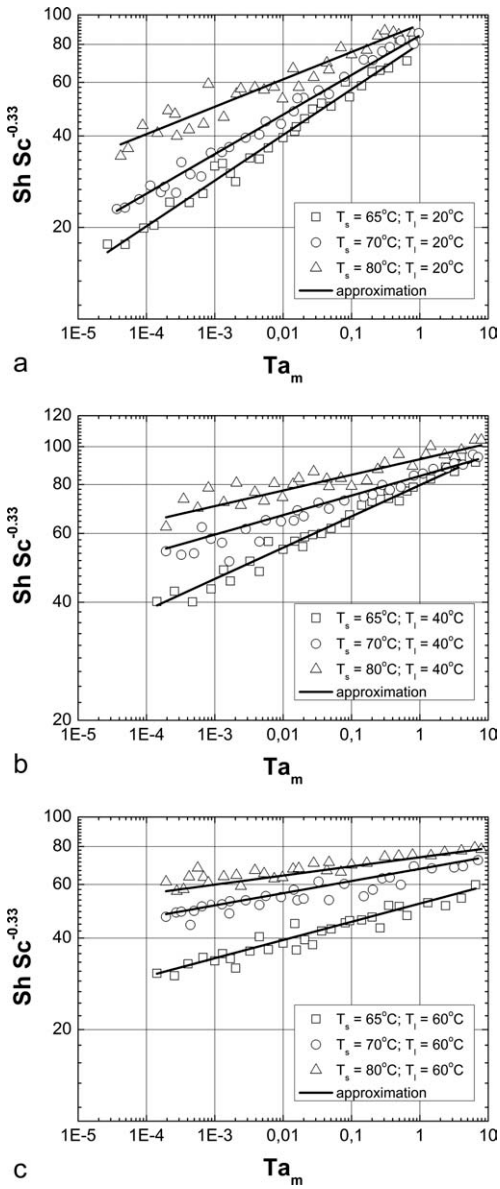


**Figure 3. The graphical presentation of mass transfer data under the action of TRMF.**

(**a**) $T_s$ = var; $T_l$ = 20°C, (**b**) $T_s$ = var; $T_l$ = 40°C, and (**c**) $T_s$ = var; $T_l$ = 60°C.

The presented results in the Figure 3 suggest that these points may be described by a unique monotonic function. The constants and exponents are computed by employing the Matlab software and the principle of least squares and the proposed relationships are collected in the Table 1.

The Figure 4 shows the effect of the constant temperature of the surface of rock-salt sample and the variation of the liquid temperature on the Sherwood number.

Figures 3 and 4 present a graphical form of the collected relations in the Table 1, as the full curves, correlated the experimental data very well with the percentage relative error ±10%. The Figure 5 gives an overview results in the form of the proposed analytical relationships for the experimental investigations (see the Table 1).

As can be clearly seen (see the Figure 3) mass transfer rates expressed as $(ShSc^{-0.33})$ increase with increasing the values of the magnetic Taylor number. It is found that as the intensity of MF increases, the velocity of liquid inside the cylindrical container increases. It may be concluded that the TRMF strongly influenced on the mass transfer process. It should be noticed that this process may be improved by means of the gradient temperature between the surface of rock-salt sample and the liquid. Figure 3 shows that Sherwood number increases with the increasing difference between the temperature of rock-salt surface and the liquid temperature. It is clear that the effect of the TRMF on the dissolution process is also depended on the temperature gradient.

Comparison of the obtained results for the analyzed process is graphically presented in Figure 4. This figure shows that for the given temperature of surface of rock-salt sample the mass transfer coefficients in tested setup are strongly depended on the values of magnetic Taylor number. These plots also confirm that the gradient temperature has significant effect on the mass transfer process. Initially, the high-mass-transfer rates are achieved by the liquid temperature 40 and 60°C. Further increase of the MF intensity leads to even higher mass transfer rates for the liquid temperature is equal to 20°C. It should be noticed that the NaCl-cylinder was placed in the middle of container. When the TRMF rotated slowly, the liquid was mixed near the wall of cylindrical container. When the TRMF rotated faster, the resulting liquid movement directly leads to an increase of the mass- and heat-transfer coefficients. This difference appears to be linked to the increase in the difference between the surface temperature of rock-salt sample and the liquid temperature associated with increasing the influence of the TRMF. The high value of the exponents of magnetic Taylor number and the multiplicative coefficients seen in the relations given in the Table 1 agree with the existence of more intensive flow near the hot surface of the rock-salt sample promoted by the increase of the magnetic induction and the temperature of the cartridge heater.

The enhancement due to heat transfer process is modeled in terms given in Eq. 39. The graphical presentation of the calculated experimental points is presented in the Figure 6.

The constant $a_3$ and exponent $b_3$ in Eq. 39 are computed by using the principle of least square. Applying the software Matlab, the analytical relationship may be obtained

**Table 1. The Developed Relationships for the Obtained Experimental Data**

| Temperature of surface of salt-rock sample | Temperature of liquid | | |
|---|---|---|---|
| | 20°C | 40°C | 60°C |
| 65°C | $\frac{Sh}{Sc^{0.33}} = 80.36\ (Ta_m)^{0.148}$ | $\frac{Sh}{Sc^{0.33}} = 79.71\ (Ta_m)^{0.08}$ | $\frac{Sh}{Sc^{0.33}} = 51.95\ (Ta_m)^{0.06}$ |
| 70°C | $\frac{Sh}{Sc^{0.33}} = 85.54\ (Ta_m)^{0.132}$ | $\frac{Sh}{Sc^{0.33}} = 84.13\ (Ta_m)^{0.05}$ | $\frac{Sh}{Sc^{0.33}} = 67.52\ (Ta_m)^{0.04}$ |
| 80°C | $\frac{Sh}{Sc^{0.33}} = 92.87\ (Ta_m)^{0.09}$ | $\frac{Sh}{Sc^{0.33}} = 92.85\ (Ta_m)^{0.04}$ | $\frac{Sh}{Sc^{0.33}} = 73.71\ (Ta_m)^{0.03}$ |

$$\frac{Sh}{Nu} = 1.5(Ta_m)^{0.12} Le^{0.33} \tag{40}$$

where the ratio of the dimensionless Sherwood and Nusselt numbers is function of the adequate dimensionless groups. The fit of experimental data with the Eq. 40 is given in the Figure 7. The averaged absolute relative error was estimated at 2.12%.

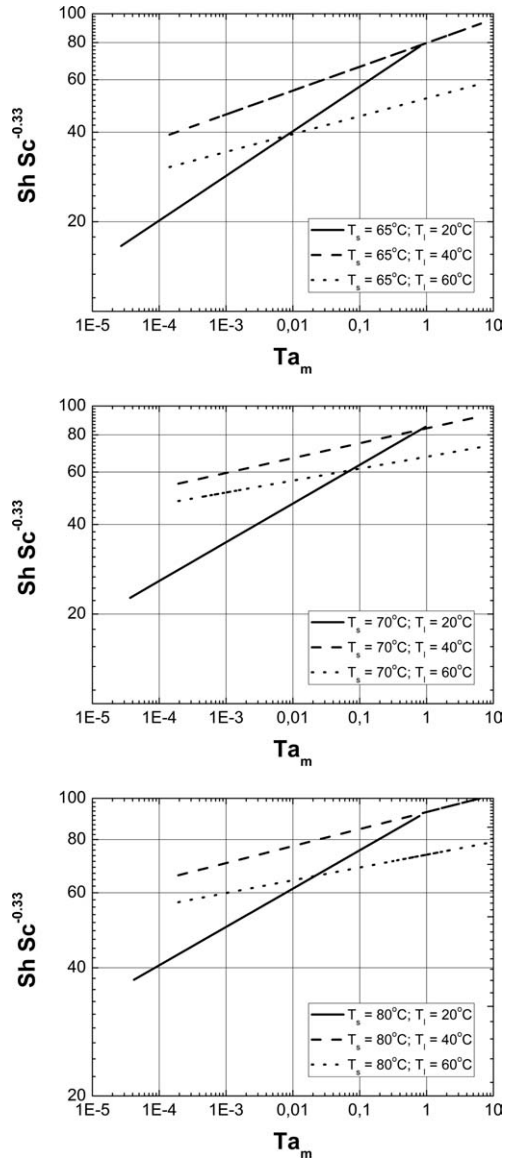


**Figure 4. The comparison of obtained results.**

(**a**) $T_s = 65°C$; $T_l =$ var, (**b**) $T_s = 70°C$; $T_l =$ var, and (**c**) $T_s = 80°C$; $T_l =$ var.

Figure 6 shows that the ratio of the mass- and heat-transfer coefficients (via ratio of Sherwood and Nusselt numbers) increases with the magnetic Taylor number. This figure shows a strong increase in mass-transfer process, when the TRMF is applied. It was found that the intensification of this process is depended on the temperature gradient between the temperature of surface of salt-rock sample and the liquid temperature.

To evaluate the influence of the gradient temperature on the mass-transfer under the action of the TRMF, the comparison between the obtained database and the empirical correlation for the dissolution process under the TRMF is presented. For comparison, these results with literature, it is recommended to correlate them under analogous form. The dissolution process under the action of the TRMF is correlated by means of the equation[3]

$$Sh = 2 + 22.5\{Ta_m\}_x^{0.015} Sc^{0.33} \left(\frac{x}{D}\right)^{0.33} \tag{41}$$

Taking into account that the dimensionless location of a NaCl-cylindrical sample $\left(\frac{x}{D}\right)$ is equal to 0.125 (the sample was located in the middle of cylindrical container), and the local Taylor number ($\{Ta_m\}_x$) is treated as the magnetic Taylor number ($Ta_m$), Eq. 41 may be rewritten in the following form

$$Sh = 2 + 11.3\{Ta_m\}_x^{0.015} Sc^{0.33}$$
$$\Rightarrow Sh_l = 2 + 11.3(Ta_m)^{0.015} Sc^{0.33} \tag{42}$$

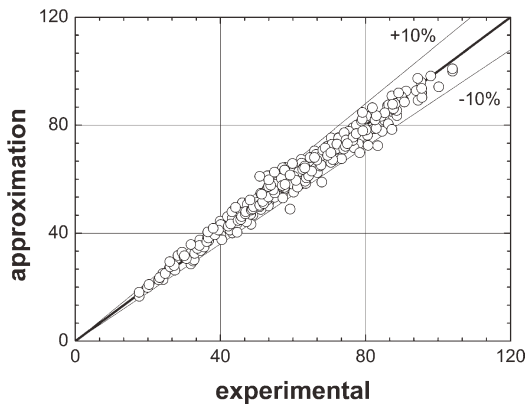


**Figure 5. Dependence between experimental and predicted $\left(\frac{Sh}{Sc^{0.33}}\right)$ values.**

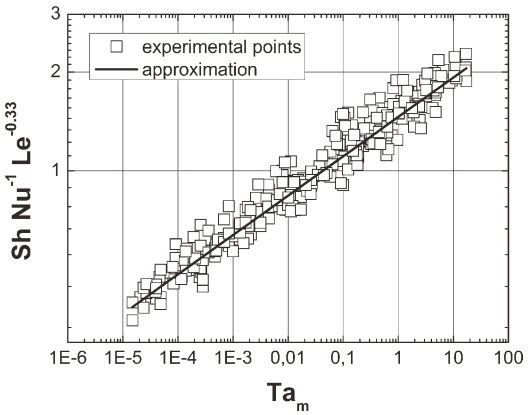


**Figure 6. The graphical presentation of mass and heat transfer data at TRMF.**

As a matter of fact, Eq. 40 may be written by alternate equations as follows

$$Sh_{II} = 1.5(Ta_m)^{0.12} Le^{0.33} Nu \tag{43}$$

The comparison in this case may be realized by considering the calculated averaged values of the dimensionless Schmidt ($[Sc]_{avg} = 477$), Lewis ($[Le]_{avg} = 74$) and Nusselt ($[Nu]_{avg} = 102$) numbers. For the established averaged values of these dimensionless groups, Eqs. 42–43 reduce to 9

$$Sh_I = 2 + 86.5(Ta_m)^{0.015} \tag{44a}$$

$$Sh_{II} = 616.3(Ta_m)^{0.12} \tag{44b}$$

The graphical comparison between Eqs. 44a and 44b is illustrated in the plot given in the Figure 8. This figure demonstrates that the dimensionless Sherwood number for the analyzed case ($Sh_{II}$) increases with increasing the magnetic Taylor number. It was found that as the intensity of the TRMF increases, the influence of hydrodynamic conditions on the transport processes inside the cylindrical container increases. The obtained relationship (Eqs. 44a–44b) indicate

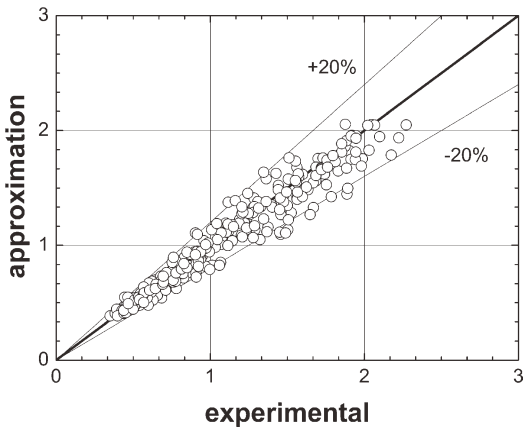


**Figure 7. Comparison of model prediction (Eq. 40) with experimental data.**

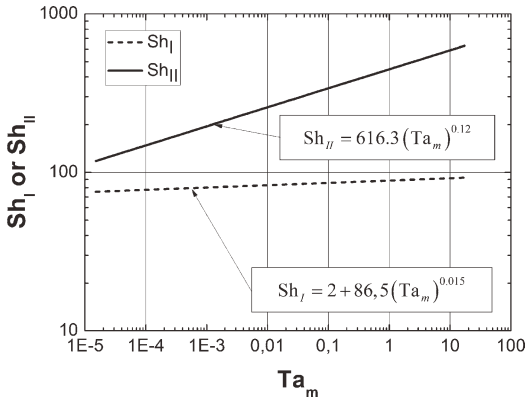


**Figure 8. Comparison of obtained results ($Sh_{II}$) with literature data ($Sh_I$).**

that the transfer rates increase with Taylor number for case I $Sh_I \sim (Ta_m)^{0.015}$ and case II $Sh_{II} \sim (Ta_m)^{0.12}$. The mass-transfer data obtained for the additional transfer gradient is consequently higher than the data obtained for the mass transfer under the action of the TRMF.

It can be observed that the enhancement of the mass transfer coefficients due to temperature gradient may be evaluated by applying the ratio $\left(\frac{Sh_{II}}{Sh_I}\right)$. In this study, $\left(\frac{Sh_{II}}{Sh_I}\right)$ becomes

$$\left(\frac{Sh_{II}}{Sh_I}\right) = \frac{616.3(Ta_m)^{0.12}}{2 + 86.5(Ta_m)^{0.015}} \Rightarrow \left(\frac{Sh_{II}}{Sh_I}\right) \approx 5(Ta_m)^{0.105} \tag{45}$$

Figure 9 shows the obtained relation (see Eq. 45) as the function of the magnetic Taylor number. It was found that as the intensity of the TRMF has strong influence on the mass transfer rate. It is interesting to note that the enhancement of this process in the case of upper values of the magnetic Taylor number is increased for the supported process by using the cartridge heater.

## Conclusions

It should be noticed that the novel approach to the mixing process presented and based on the application of TRMF to produce better hydrodynamic conditions in the case of the mass-transfer process. From practical point of view, the

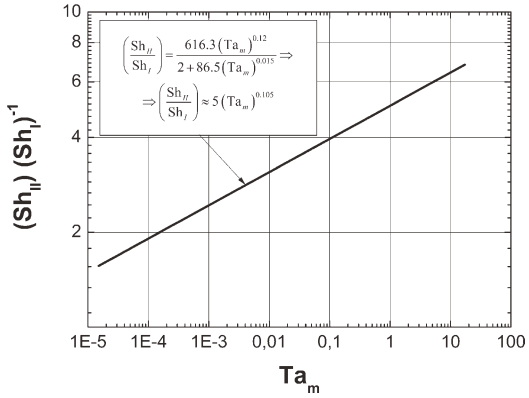


**Figure 9. Graphical presentation of Eq. 45.**

dissolution process of solid body is involved by using the turbulently agitated systems. In previous publications, there were no available data describing the mass-transfer operations of the dissolution process under the TRMF conditions and the temperature gradient. Therefore, the experimental investigations have been conducted to explain the influence of this kind of MF on the mass-transfer enhancement. Moreover, the influence of the additional indirect heating on the mass-transfer was determined. The influence of the TRMF and the temperature gradient on this process is described using the nondimensional parameters formulated on the base of fluid mechanics equations. These dimensionless numbers allow quantitative representation and characterization of the influence of hydrodynamic state under the TRMF conditions on the mass-transfer process. The dimensionless groups are used to establish the effect of the TRMF on this operation in the form of the novel type dimensionless correlation.

## Notation

$\overline{B}$ = magnetic induction, kg $A^{-1}$ $s^{-2}$
$c_i$ = concentration, $kg_i$ $kg^{-1}$
$c_p$ = specific heat capacity of liquid, J $kg^{-1}deg^{-1}$
$d_s$ = sample diameter, m
$D$ = diameter of container, m
$D_i$ = diffusion coefficient, $m^2$ $s^{-1}$
$D_m$ = magnetic diffusion, $m^2$ $s^{-1}$
$f_{TRMF}$ = frequency of electrical current (equal to frequency of TRMF), $s^{-1}$
$F_m$ = cylindrical surface of dissoluble sample, $m^2$
$\overline{F_{em}}$ = Lorenz magnetic force, N
$h_s$ = length of sample, m
$l$ = characteristic dimension, m
$\overline{J}$ = electrical current density vector, A $m^{-2}$
$\overline{J_i}$ = flux density of component $i$, $kg_i$ $m^{-3}$ $s^{-1}$
$\overline{J_{dyf}}$ = diffusion flux density, $kg_i$ $m^{-3}$ $s^{-1}$
$k_{\overline{F_{em}}}$ = relative coefficient of diffusion resulting from additional forced interactions (e.g. magnetic field), $kg_i$ $m^{-1}$ $^{-1}$ $\left(kg_i\ s^2\ m^{-2}\ kg^{-1}\right)$
$m_i$ = mass of dissoluble NaCl sample, $kg_{NaCl}$
$Q_l$ = heat flow from liquid, W
$Q_s$ = heat flow from sample, W
$T$ = temperature, deg
$[T_l]_{t_1}$ = temperature of liquid at moment $t_1$, deg
$[T_l]_{t_2}$ = temperature of liquid at moment $t_2$ (after time of dissolution process), deg
$T_s$ = temperature of sample, deg
$V$ = volume of liquid, $m^3$
$\overline{w}$ = velocity, $m{\cdot}s^{-1}$
$\overline{w_i}$ = velocity of component $i$, m $s^{-1}$
$x$ = distance (for localization of sample), m

### Greek letter

$\alpha_s$ = heat transfer coefficient, W $m^{-2}$ $deg^{-1}$
$\beta_i$ = mass transfer coefficient, $kg_i$ $m^{-2}$ $s^{-1}$
$\eta$ = dynamic viscosity, kg $m^{-1}$ $s^{-1}$
$\mu_m$ = magnetic permeability, kg m $A^{-2}$ $s^{-2}$
$\lambda$ = thermal conductivity of liquid, W $m^{-1}$ $deg^{-1}$
$\nu$ = kinematic viscosity, $m^2$ $s^{-1}$
$\nu_m$ = magnetic viscosity, $m^2$ $s^{-1}$
$\rho$ = density, kg $m^{-3}$
$\rho_i$ = concentration of component $i$, $kg_i$ $m^{-3}$
$\sigma_e$ = electrical conductivity, $A^2$ $s^3$ $kg^{-1}$ $m^{-3}$
$\tau$ = time dissolution or time, s
$\Phi_i$ = mass flux of component $i$, $kg_i$ $m^{-3}$ $s^{-1}$
$\omega_{TRMF}$ = angular velocity of transverse rotating magnetic field, rad $s^{-1}$

### Subscripts

avg = averaged value
$l$ = liquid
$s$ = sample
0 = reference value

### Abbreviation

AC = alternating current
MF = magnetic field
TRMF = transverse rotating magnetic field

### Dimensionless numbers

$Ha = B_0 l_0 \sqrt{\frac{\sigma_{e_0}}{\nu \rho_0}}$ = Hartman number
$Le = \frac{a}{D_i}$ = Lewis number
$Nu = \frac{[\alpha_s]_{\text{avg}} D}{\lambda}$ = Nusselt number
$Pe_i = \frac{l_0 w_0}{D_{i_0}}$ = mass Peclet number
$Pr_m = \frac{\nu}{\nu_{m_0}}$ = magnetic Prandtl number
$Q = \frac{\sigma_{e_0} B_0^2 l_0^2}{\nu \rho_0}$ = Chandrasekhar number
$Re = \frac{w_0 D}{\nu}$ = Reynols number
$S = \frac{\tau_0 w_0}{l_0}$ = Strouhal number
$Sc_i = \frac{\nu}{D_{i_0}}$ = Schmidt number
$Sh = \frac{\left[(\beta_i)_V\right]_0 d_p^2}{\rho_0 D_{i_0}}$ = Sherwood number
$Ta_m = \frac{w_0 \sigma_{e_0} B_0^2 l_0^3}{\nu^2 \rho_0}$ = magnetic Taylor number

## Literature Cited


1. Basmadjian D. *Mass Transfer: Principles and Applications*. Boca Raton: CRC Press LLC, 2004.
2. Rakoczy R, Masiuk S. Influence of transverse rotating magnetic field on enhancement of solid dissolution process. *AIChE J*. 2010;56:1416–1433.
3. Rakoczy R. Enhancement of solid dissolution process under the influence of rotating magnetic field. *Chem Eng Process Process Intensif*. 2010;49:42–50.
4. Volz MP, Mazuruk K. Thermoconvective instability in a rotating magnetic field. *Int J Heat Mass Transf*. 1999;42:1037–1045.
5. Melle S, Calderon OG, Fuller GG, Rubio MA. Polarizable particle aggregation under rotating magnetic fields using scattering dichroism. *J Colloid Interface Sci*. 2002;247:200–209.
6. Walker JS, Volz MP, Mazuruk K. Rayleigh-Bénard instability in a vertical cylinder with a rotating magnetic field. *Int J Heat Mass Transf*. 2004;47:1877–1887.
7. Nikrityuk PA, Eckert K, Grundmann R. A numerical study of unidirectional solidification of a binary metal alloy under influence of a rotating magnetic field. *Int J Heat Mass Transf*. 2006;49:1501–1515.
8. Yang M, Ma N, Bliss DF, Bryant GG. Melt motion during liquid-encapsulated Czochralski crystal growth in steady and rotating magnetic field. *Int J Heat Mass Transf*. 2007;28:768–776.
9. Fraňa K, Stiller J, Grundmann R. Transitional and turbulent flows driven by a rotating magnetic field. *Magnetohydrodynamics*. 2006;42:187–197.
10. Spitzer KH. Application of rotating magnetic field in Czochralski crystal growth. *Progr Cryst Growth Char Mater*. 1999;38:39–58.
11. Hristov J. Simple bed expansion correlations for magnetically assisted gas-fluidized tapered beds. *Int Rev Chem Eng*. 2009;1:316–323.
12. Fu MJ, Arifin NM, Nazar R, Saad MN. Effect of non-uniform temperature gradient and magnetic field on Marangoni convection in a micropolar fluid. *Int Rev Chem Eng*. 2009;1:369–374.
13. Abbasov T, Yildiz Z, Sarimeseli A. An experimental study on impacts of some process parameters on the electromagnetic filtration performance. *Int Rev Chem Eng*. 2010;2:289–292.

14. Hristov J. Magnetic field assisted fluidization—a unified approach. Part 3. Heat transfer in gas-solid fluidized beds—a critical re-evaluation of the results. *Rev Chem Eng*. 2003;19:229–355.
15. Hristov J. Magnetic field assisted fluidization—a unified approach. Part 7. Mass transfer: chemical reactors, basic studies and practical implementations thereof. *Rev Chem Eng*. 2009;25:1–254.
16. Al-Qodah Z, Al-Bisoul M, Al-Hassan M. Hydro-thermal behavior of magnetically stabilized fluidized beds. *Powder Technol*. 2001;115:58–67.
17. Aksielrud GA, Mołczanow AD. *Dissolution Process of Solid Bodies*. Warsaw: WNT, 1981.
18. Incropera FP, DeWitt DP. *Fundamentals of Heat and Mass Transfer*. New York: Wiley, 1996.
19. Kays WM, Crawford ME. *Convective Heat and Mass Transfer*. New York: McGraw-Hill, 1993.
20. Bird RB, Stewart WE, Lightfoot EN. *Transport Phenomena*. New York: Wiley, 2002.
21. Garner FH, Suckling RD. Mass transfer form a soluble solid sphere. *AIChE J*. 1958;4:14–124.
22. Noordsij P, Rotte JW. Mass transfer coefficients to a rotating and to a vibrating sphere. *Chem Eng Sci*. 1967;22:1475–1481.
23. Jameson GJ. Mass (or heat) transfer from an oscillating cylinder. *Chem Eng Sci*. 1964;19:793–800.
24. Condoret JS, Riba JP, Angelino H. Mass transfer in a particle bed with oscillating flow. *Chem Eng Sci*. 1989;44:2107–2111.
25. Tojo K, Miyanami K, Mitsui H. Vibratory agitation in solid-liquid mixing. *Chem Eng Sci*. 1981;36:279–284.
26. Lemcoff NO, Jameson GJ. Solid-liquid mass transfer in a resonant bubble contractor. *Chem Eng Sci*. 1975;30:363–367.
27. Sugano Y, Rutkowsky DA. Effect of transverse vibration upon the rate of mass transfer for horizontal cylinder. *Chem Eng Sci*. 1968;23:707–716.
28. Wong PFY, Ko NWM, Yip PC. Mass transfer from large diameter vibrating cylinder. *Trans Item*. 1978;56:214–216.
29. Lemlich R, Levy MR. The effect of vibration on natural convective mass transfer. *AIChE J*. 1961;7:240–241.
30. Rakoczy R, Masiuk S. Experimental study of bubble size distribution in a liquid column exposed to a rotating magnetic field. *Chem Eng Process Process Intensif*. 2009;48:1229–1240.

*Manuscript received Dec. 4, 2010, revision received Feb. 28, 2011, and final revision received Apr. 11, 2011.*